Effects of the alkyl-chain length on the mixing state of imidazolium-based ionic liquid-methanol solutions

ARTICLE *in* PHYSICAL CHEMISTRY CHEMICAL PHYSICS · OCTOBER 2010

Impact Factor: 4.49 · DOI: 10.1039/c0cp00614a · Source: PubMed

3 AUTHORS, INCLUDING:

Kenta Fujii
Yamaguchi University
83 PUBLICATIONS **1,758** CITATIONS
SEE PROFILE

Toshiyuki Takamuku
Saga University
84 PUBLICATIONS **1,930** CITATIONS
SEE PROFILE

Effects of the alkyl-chain length on the mixing state of imidazolium-based ionic liquid–methanol solutions

Takuya Shimomura, Kenta Fujii† and Toshiyuki Takamuku*

Received 19th May 2010, Accepted 14th July 2010
DOI: 10.1039/c0cp00614a

Effects of the alkyl-chain length of the imidazolium cation on the mixing state of imidazolium-based ionic liquids, 1-alkyl-3-methylimidazolium ($C_n$mim$^+$, the alkyl-chain lengths n of 4, 6, 8, 10, and 12) bis(trifluoromethanesulfonyl)amide (TFSA$^-$), and methanol were investigated using small-angle neutron scattering (SANS), attenuated total reflectance infrared (ATR-IR), and NMR techniques. SANS measurements revealed that $C_n$mim$^+$TFSA$^-$ is heterogeneously mixed with methanol in the methanol mole fraction range of $0.8 \leq x_{CD_3OD} \leq 0.995$. The heterogeneity of the $C_n$mim$^+$TFSA$^-$–methanol solutions, except for C_4mim$^+$TFSA$^-$, is most enhanced at $x_{CD_3OD} \approx 0.97$ over the entire mole fraction range. Thus, the mole fraction at the maximum heterogeneity of the solutions is independent of the alkyl-chain length. In contrast, the magnitude of the maximum heterogeneity of the solutions is larger in the order of the alkyl-chain length from $n = 4$ to 12. ATR-IR and NMR measurements showed that methanol molecules gradually form hydrogen bonds among them in the solutions with increasing x_{CH_3OH}. In particular, the hydrogen-bonds among methanol molecules are conspicuously evolved in the solutions above $x_{CH_3OH} \approx 0.8$. The increase in the concentration of the hydrogen-bonded methanol with increasing x_{CH_3OH} does not significantly depend on the alkyl-chain length. According to these results, we concluded that the heterogeneity of $C_n$mim$^+$TFSA$^-$–methanol solutions arises from polar domains composed of the imidazolium rings, TFSA$^-$, and methanol clusters and nonpolar domains formed by interaction among the alkyl chains of the imidazolium cations.

1. Introduction

Ionic liquids (ILs) have unique properties, such as extremely low vapor pressure, thermal stability, nonflammability, high polarity, and electroconductivity. Hence, ILs have been investigated as novel solvents in various fields of organic synthesis, catalysis, electrochemistry, and material separation, such as high performance liquid chromatography (HPLC) and liquid–liquid extraction.[1–7] In such researches, ILs are frequently used by mixing with conventional molecular liquids to change their physicochemical properties, such as viscosity, polarity, and conductivity.[2,8–11] Properties of IL–molecular liquid solutions should arise from their mixing state at the molecular level.

Many researchers have focused on 1-alkyl-3-methylimidazolium ($C_n$mim$^+$)-based ionic liquids to elucidate changes in the properties of the ILs with varying the alkyl-chain length n. Lopes and Pádua have performed molecular dynamics (MD) simulations to clarify nanometre-scale structure of $C_n$mim$^+$PF$_6^-$ and $C_n$mim$^+$ bis(trifluoromethanesulfonyl)-amide (TFSA$^-$) with $n = 2$–12.[12] They have concluded that microphase separation between polar domains and nonpolar domains occurs in the ILs: the polar domain consists of the positively charged imidazolium rings and anions, while the nonpolar domain is formed by interaction among the alkyl chains of the imidazolium cations. The longer the alkyl chain, the more the microphase separation progresses in the ILs. Triolo *et al.* have conducted small-angle X-ray scattering (SAXS) measurements on $C_n$mim$^+$Cl$^-$ and $C_n$mim$^+$BF$_4^-$ at 298 K with varying the alkyl-chain length from $n = 3$ to 10.[13] A peak appears at the momentum transfer q of $\sim$2.5 nm^{-1} in SAXS spectra of the ILs. The intensity of the peak strengthens and its position shifts to the low q as the alkyl chain is elongated. Based on these experimental results, they have concluded microphase separation due to the formation of polar and nonpolar domains and the growth of the nonpolar domains with increasing the chain length.

For IL–molecular liquid solutions, Lopes *et al.* have clarified interactions between C_4mim$^+$PF$_6^-$ and *n*-hexane, acetonitrile, water, and methanol using MD simulations.[14,15] The MD results have shown that *n*-hexane molecules favorably interact with the alkyl chain of the imidazolium cation, while water and methanol form hydrogen bonds with the imidazolium hydrogen atoms and the fluorine atoms of PF$_6^-$. Acetonitrile molecules can interact with both the imidazolium hydrogen atoms and the alkyl chain. Voth *et al.* have succeeded in visualising the loosening of the polar and nonpolar domains in C_8mim$^+$NO$_3^-$ by addition of water using MD simulations.[16] In the water mole fraction range of $x_{H_2O} < \sim 0.8$, water molecules are hydrogen-bonded with the oxygen atoms of nitrate ion in the polar domains. As the water content further increases, the electrostatic interaction between

Department of Chemistry and Applied Chemistry, Graduate School of Science and Engineering, Saga University, Honjo-machi, Saga 840-8502, Japan. E-mail: takamut@cc.saga-u.ac.jp
† Present address: Neutron Science Laboratory, Institute for Solid State Physics, The University of Tokyo, Kashiwanoha 5-1-5, Kashiwa 277-8581, Japan.

C_8mim^+ and NO_3^- is weakened by intruding water clusters enhanced around nitrate ions. Thus, the polar domains are disrupted. This induces the weakening of the hydrophobic interaction among the alkyl groups in the nonpolar domains.

Experimental techniques have also been adopted to investigate IL–molecular liquid solutions. In aqueous solutions, imidazolium-based ILs may form micelles.[11,17–20] Bowers *et al*. have observed aggregation behaviour of $C_4mim^+BF_4^-$, $C_8mim^+Cl^-$, and $C_8mim^+I^-$ in their aqueous solutions by surface tension, conductivity, and small-angle neutron scattering (SANS) measurements.[17] Investigations on liquid–liquid equilibria of imidazolium-based IL–alcohol solutions[21,22] have revealed that an upper critical solution temperature (UCST) of the solutions decreases with increasing the alkyl-chain length of the imidazolium cation. Thus, the mixing state of imidazolium-based IL–alcohol solutions definitely depends on the alkyl-chain length. We have performed SANS experiments on methanol and acetonitrile solutions of $C_2mim^+Cl^-$ and methanol and benzene solutions of $C_2mim^+TFSA^-$ at several mole fractions of the molecular liquids.[23] These results showed that $C_2mim^+Cl^-$ and $C_2mim^+TFSA^-$ aggregate in acetonitrile and methanol solutions, respectively. However, exact concentrations of the maximum aggregation have not been determined.

Despite these efforts on IL–molecular liquid solutions, influences of the alkyl-chain length on the mixing state of imidazolium-based IL and molecular liquids at the molecular level have not been systematically and directly clarified using experimental techniques, such as X-ray and neutron scattering methods. In particular, the loosening of the polar and nonpolar domains by addition of molecular liquid has not yet been corroborated by experimental results.

In the present investigation, we chose $C_nmim^+TFSA^-$ with n = 4, 6, 8, 10, and 12 (Fig. 1). Methanol was adopted as cosolvent because methanol is the simplest nonaqueous solvent and these ILs can be mixed with methanol at any ratio. SANS measurements at 298 K were carried out on $C_nmim^+TFSA^-$–CD_3OD solutions to observe the heterogeneity of the solutions at various methanol mole fractions x_{CD_3OD}. In addition, attenuated total reflectance infrared (ATR-IR) measurements were conducted on $C_nmim^+TFSA^-$–CH_3OH solutions with varying x_{CH_3OH}. The concentrations of isolated and hydrogen-bonded methanol molecules of the solutions were determined from the O–H vibration bands of methanol. To clarify the mixing state of $C_nmim^+TFSA^-$–CH_3OH solutions in terms of electron densities of the hydrogen and carbon atoms of ILs and methanol, ^1H and ^{13}C NMR spectra of the solutions were recorded at 298 K. According to all the results, effects of the alkyl-chain length on the mixing state of $C_nmim^+TFSA^-$–methanol solutions are discussed at the molecular level.

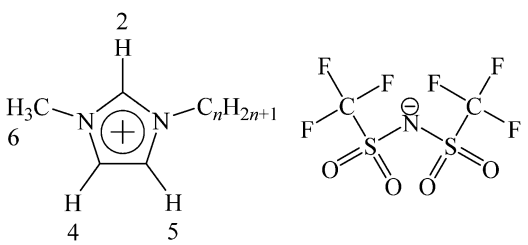

Fig. 1 Structure of $C_nmim^+TFSA^-$ with the position-numbers of the hydrogen and carbon atoms.

2. Experimental

Reagents

$C_nmim^+TFSA^-$ (n = 4, 6, 8, 10, and 12) were synthesised according to the conventional method previously reported.[24] Water contents of $C_nmim^+TFSA^-$ were estimated to be less than 300 ppm by a Karl-Fischer titration. Deuterated methanol, CD_3OD (Cambridge Isotope Laboratories, D content = 99.8%), was used for SANS experiments to contrast CD_3OD with undeuterated $C_nmim^+TFSA^-$ due to the largely different scattering lengths of D and H atoms (6.67 and −3.74 fm, respectively). CH_3OH (Wako Pure Chemicals, grade for HPLC) was adopted for ATR-IR and ^1H and ^{13}C NMR experiments.

Sample solutions

Sample solutions for SANS experiments were prepared by weighing $C_nmim^+TFSA^-$ and CD_3OD at required x_{CD_3OD} under a dry nitrogen atmosphere in a glove-box to avoid moisture and replacement of D atoms of CD_3OD with H atoms. Compositions of the sample solutions for SANS experiments are listed in Table 1. $C_nmim^+TFSA^-$–CH_3OH solutions for ATR-IR and ^1H and ^{13}C NMR experiments were prepared in the x_{CH_3OH} range from 0 to 0.99. Densities of the sample solutions were measured at 298.2 K with an electronic densimeter (Anton Paar GmbH, DSA5000) for the analysis of SANS and ATR-IR data.

SANS experiments

SANS experiments were conducted on the $C_nmim^+TFSA^-$–CD_3OD solutions using the SANS-U spectrometer installed at reactor JRR-3M in the Japan Atomic Energy Agency (JAEA), Tokai, Japan. The sample solutions were kept in a quartz cell of 10 mm in width, 40 mm in height, and 2 mm in sample thickness. The temperature of the solutions was controlled at 298.2 ± 0.1 K. The wavelength of incident neutron beam was λ = 0.70 nm. A two-dimensional position-sensitive detector was placed at camera lengths of 1 and 4 m to cover the momentum transfer q ($= 4\pi\lambda^{-1}\sin\theta$) range of 0.15–3.0 nm^{-1}.[25,26] The scattering intensities from the sample solution were collected with the detector at the camera lengths of 1 and 4 m for 10 min and 1 h, respectively. The observed intensities were corrected for background by subtraction of intensities of an empty cell, and then normalised by dividing the intensities for each sample solution by those for F200-0, a standard low density polyethylene.

ATR-IR spectroscopy

ATR-IR experiments with a single reflectance were carried out on the $C_nmim^+TFSA^-$–CH_3OH solutions over the entire x_{CH_3OH} range at room temperature using an FT-IR spectrometer (JASCO, FT/IR-6100) equipped with ATR diamond prism (JASCO, PKS-D 470 with ATR PRO450-S). During the

Table 1 Mole fractions x_{CD_3OD} and volume fractions ϕ_{CD_3OD} of methanol for $C_n$mim$^+$TFSA$^-$–CD_3OD solutions and their Ornstein–Zernike correlation lengths (ξ/nm) determined by SANS experiments[a]

C_4mim$^+$TFSA$^-$–CD_3OD			C_6mim$^+$TFSA$^-$–CD_3OD			C_8mim$^+$TFSA$^-$–CD_3OD			C_{10}mim$^+$TFSA$^-$–CD_3OD			C_{12}mim$^+$TFSA$^-$–CD_3OD		
x_{CD_3OD}	ϕ_{CD_3OD}	ξ	x_{CD_3OD}	ϕ_{CD_3OD}	ξ	x_{CD_3OD}	ϕ_{CD_3OD}	ξ	x_{CD_3OD}	ϕ_{CD_3OD}	ξ	x_{CD_3OD}	ϕ_{CD_3OD}	ξ
0.500	0.122		0.500	0.111		0.500	0.102		0.501	0.0937		0.502	0.0874	
0.601	0.173		0.600	0.158		0.600	0.145		0.600	0.134		0.600	0.125	
0.700	0.245		0.701	0.226		0.700	0.209		0.700	0.194		0.700	0.182	
0.800	0.358	0.11(1)	0.800	0.333	0.06(1)	0.800	0.311		0.800	0.292		0.800	0.276	
0.900	0.556	0.18(1)	0.900	0.529	0.15(1)	0.900	0.504	0.14(1)	0.900	0.482	0.13(1)	0.900	0.461	0.17(1)
0.950	0.726	0.19(1)	0.950	0.703	0.19(1)	0.950	0.682	0.20(1)	0.950	0.662	0.20(1)	0.950	0.644	0.25(1)
0.970	0.818	0.18(1)	0.970	0.807	0.20(1)	0.970	0.785	0.21(1)	0.970	0.770	0.23(1)	0.970	0.755	0.26(1)
0.990	0.933	0.12(1)	0.990	0.925	0.15(1)	0.990	0.918	0.18(1)	0.990	0.911	0.20(1)	0.990	0.904	0.21(1)
									0.995	0.954	0.14(1)	0.995	0.950	0.17(1)

[a] The values in parentheses are standard deviations of the last figures.

measurements, the light path in the spectrometer was purged with dry N_2 gas at a flow rate of 5 dm^3 min^{-1} to eliminate moisture and carbon dioxide. The absorption spectra were accumulated for 64 times per sample with a resolution of 4.0 cm^{-1}. In the ATR-IR spectroscopy, the absorption occurs in the evanescent wave penetrating into the sample, resulting in a decrease in the amplitude of irradiated light. The penetration depth d_p of the evanescent wave per reflection by a prism can be estimated through[27]

$$d_p = \frac{\lambda}{2\pi}\left(n_1\sqrt{\sin^2\theta - n_2^2/n_1^2}\right)^{-1}. \quad (1)$$

Here, λ represents the wavelength of the light, θ is the incident angle (45°), n_1 and n_2 are the refractive indexes of diamond prism (2.42) and sample solution, respectively. Thus, the wavelength dependence of the penetration depth must be corrected to exactly determine the peak area for each absorption band. In the present experiments, the reflective indexes of the samples at 298 K were determined using a digital Abbe refractometer (ATAGO, DR-A1) to correct the path length of the light for the spectra.

NMR spectroscopy

^{1}H and ^{13}C NMR spectra of the $C_n$mim$^+$TFSA$^-$–CH_3OH solutions were recorded at 298 K on an FT-NMR spectrometer (JEOL, JNM-AL300). An external double reference tube (Shigemi), which has a capillary shape with a blown-up sphere at its base, was inserted into the sample tube (Shigemi, PS-001-7). Hexamethyldisiloxane (HMDS) (Wako Pure Chemicals, the first purity grade) was used as a reference substance for ^{1}H and ^{13}C atoms. The observed chemical shifts were corrected for the volume magnetic susceptibility of a sample solution using an external double reference method as described below.[28–31] A couple of NMR signals of the reference substance at the sphere and capillary parts is observed in an NMR spectrum. The difference in the chemical shifts between the two parts, $\Delta\delta_{ref}$/ppm, is related to the volume magnetic susceptibility of a sample solution χ_s and the reference substance χ_r as

$$\Delta\delta_{ref} = \kappa(\chi_s - \chi_r) \times 10^6, \quad (2)$$

where κ denotes the shape factor for the reference tube. The κ value has been determined in advance of sample measurements from the $\Delta\delta_{ref}$ data for $CDCl_3$, $(CD_3)_2SO$, C_6D_{12}, C_6D_6, and $(CD_3)_2CO$ measured at 298 K, as their χ_s values are available from the literature.[28] Hence, the diamagnetic effect of a sample solution on the reference substance can be corrected on the observed chemical shift δ_{obs} through

$$\delta_{corr} = \delta_{obs} - (4\pi/3)(\chi_s - \chi_r) \times 10^6 = \delta_{obs} - (4\pi/3\kappa)\Delta\delta_{ref}, \quad (3)$$

where the δ_{obs} value is the shift from the reference signal of the capillary part.

3. Results and discussion

SANS experiments

Fig. 2 shows neutron scattering intensities of the $C_n$mim$^+$TFSA$^-$–CD_3OD solutions with n = 4–12 at various x_{CD_3OD}. For the solutions with n = 4–8 below x_{CD_3OD} = 0.7 (volume fraction ϕ_{CD_3OD} of ~0.2), the intensities rise at the high q side. In the spectra of the C_{12}mim$^+$TFSA$^-$–CD_3OD, a peak appears at q = 2.2 nm^{-1}. As shown by the SAXS measurements,[13] these features arise from the inherent interactions in pure ILs. In fact, the intensity of the peak decreases with decreasing IL content. For all the solutions below x_{CD_3OD} = 0.7, significant SANS intensities are not observed. This suggests thus that methanol molecules are embedded into the inherent structure of $C_n$mim$^+$TFSA$^-$ in the range of $x_{CD_3OD} \leq 0.7$. The SANS intensities of the $C_n$mim$^+$TFSA$^-$–CD_3OD solutions gradually rise with increasing x_{CD_3OD} from 0.8 ($\phi_{CD_3OD} \approx 0.3$) to 0.97 ($\phi_{CD_3OD} \approx 0.8$), showing that the concentration fluctuation of the solutions is gradually enhanced. However, the SANS intensities of the solutions are decreased at x_{CD_3OD} = 0.99. These findings reveal that the mixing state of $C_n$mim$^+$TFSA$^-$ and methanol molecules is the most heterogeneous in the solutions at $x_{CD_3OD} \approx 0.97$.

To evaluate the heterogeneity of the $C_n$mim$^+$TFSA$^-$–CD_3OD solutions, the SANS intensities above x_{CD_3OD} = 0.8 or 0.9 were fitted by a least-squares refinement procedure through the Ornstein–Zernike equation,

$$I(q) = \frac{I_0}{1 + \xi^2 q^2} + \text{B.G.}, \quad (4)$$

where I_0 is the scattering intensity at q = 0, ξ and B.G. represent the Ornstein–Zernike correlation length and

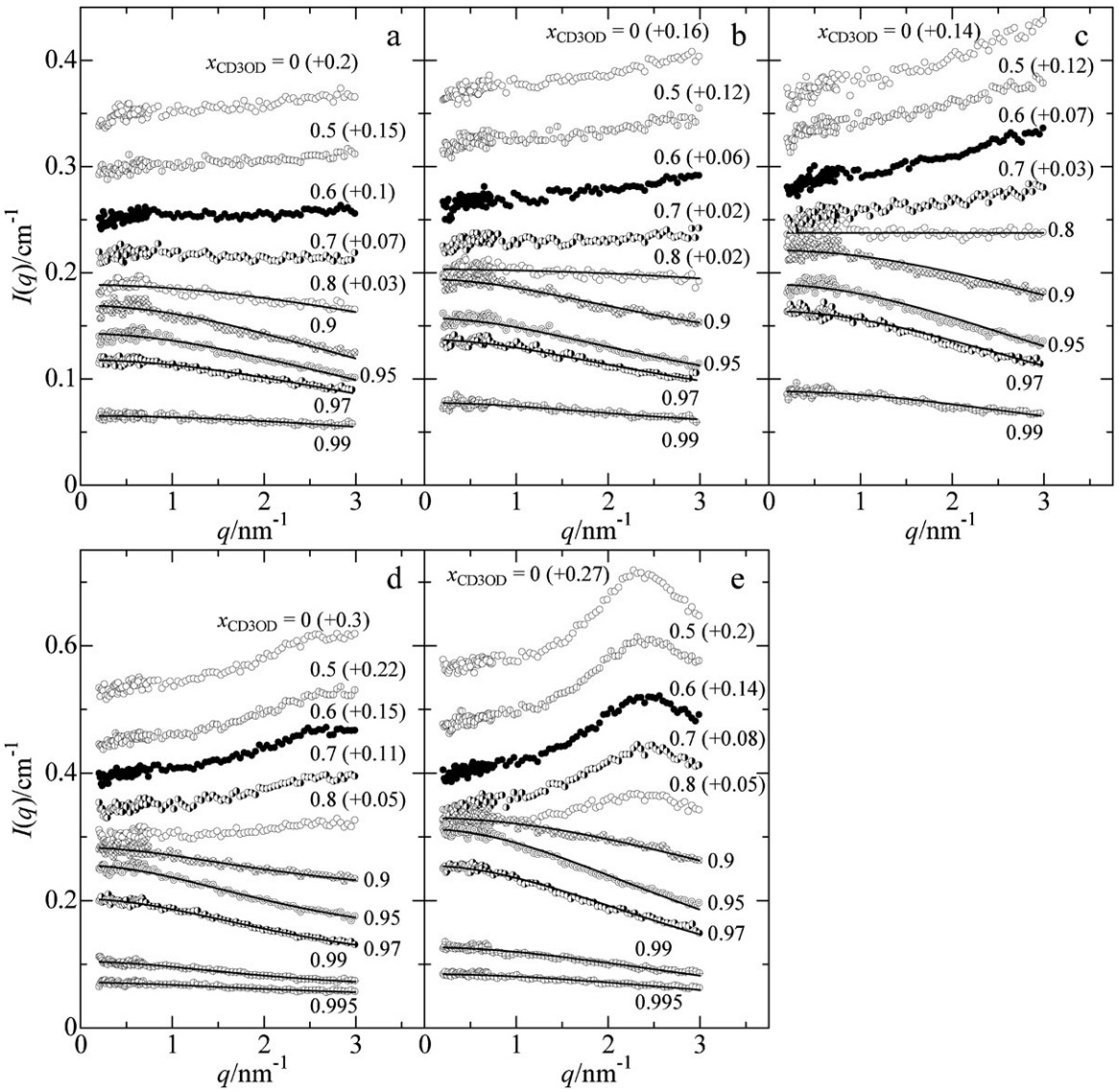

Fig. 2 SANS intensities of $C_n$mim$^+$TFSA$^-$–CD_3OD solutions at various CD_3OD mole fractions ((a) n = 4; (b) 6; (c) 8; (d) 10; (e) 12). The values in parentheses are those shifted from the origin to avoid overlap of the plots. The solid lines show the results of least-squares fits using eqn (4).

background intensities, respectively. The theoretical values (solid lines, Fig. 2) obtained by the least-squares fits well reproduce the observed ones. The Ornstein–Zernike correlation lengths ξ determined are listed in Table 1 and plotted as a function of x_{CD_3OD} in Fig. 3. The ξ values of the C_4mim$^+$TFSA$^-$–CD_3OD solutions increase with increasing x_{CD_3OD} and reach a maximum at x_{CD_3OD} = 0.95. In contrast, a maximum of the ξ of the $C_n$mim$^+$TFSA$^-$–CD_3OD solutions with n = 6–12 appears at the higher mole fraction of x_{CD_3OD} = 0.97. Thus, the mole fraction at the maximum ξ is independent of the alkyl-chain length of the imidazolium cation, except for C_4mim$^+$. This finding suggests that hydrogen bonding among methanol molecules mainly governs the heterogeneous mixing state of the ILs and methanol. However, the maximum ξ value of the solutions increases with increasing the alkyl-chain length.

Fig. 3 reveals that heterogeneous mixing of the solutions is observed in the very narrow range of $0.8 \leq x_{CD_3OD} \leq 0.995$. This is comparable with the mixing state of C_4mim$^+$$BF_4^-$–$D_2O$ solutions reported by Almásy *et al.*[32] The ξ values and the Kirkwood–Buff integral values determined by SANS experiments on C_4mim$^+$$BF_4^-$–$D_2O$ solutions showed that C_4mim$^+$$BF_4^-$ and D_2O are heterogeneously mixed with each other in the water mole fraction range of $0.84 \leq x_{D_2O} \leq 0.99$ with a maximum at x_{D_2O} = 0.93. The maximum ξ value (0.19 nm) of the C_4mim$^+$TFSA$^-$–CD_3OD solutions is smaller by a factor of $\sim$7 than that (1.41 nm) of C_4mim$^+$$BF_4^-$–$D_2O$ solutions, *i.e.*, the heterogeneity of the former is less. This is attributed to the higher hydrophobicity of methanol than water. Indeed, phase separation of C_4mim$^+$$BF_4^-$–water solutions occurs below $\sim$20 K from room temperature,[32] while the C_4mim$^+$TFSA$^-$–methanol solutions do not separate by cooling at least until 273 K.

ATR-IR spectroscopy

Fig. 4 shows representative ATR-IR spectra of the C_{12}mim$^+$TFSA$^-$–CH_3OH solutions in the wavenumber range

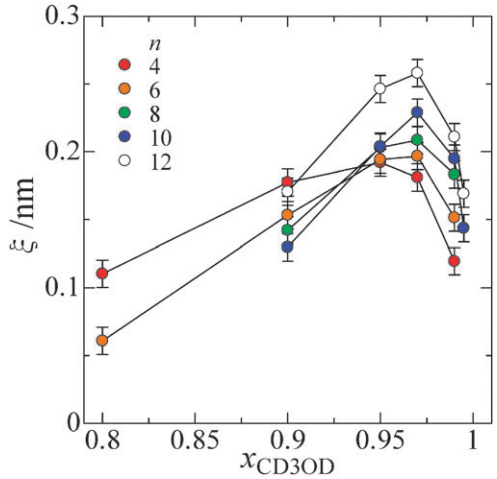

Fig. 3 Ornstein–Zernike correlation lengths ξ of $C_n mim^+TFSA^-$–CD_3OD solutions as a function of CD_3OD mole fraction. The standard deviations σ are indicated as error bars.

from 2600 to 3800 cm^{-1}. The spectra were corrected for the wavelength dependence of the path length using eqn (1). In the spectrum of pure $C_{12}mim^+TFSA^-$ ($x_{CH_3OH} = 0$), three small peaks at 3096, 3121, and 3158 cm^{-1} are attributed to the asymmetric C–H vibration of the methyl groups and the C_2–H and $C_{4,5}$–H vibrations of the imidazolium ring, respectively.[33–35] Large and sharp peaks at 2856 and 2926 cm^{-1} and a shoulder at 2957 cm^{-1} arise from various C–H vibrations of both methyl and dodecyl groups.[33–35] In the spectrum of pure methanol ($x_{CH_3OH} = 1$), four peaks at 2830, 2913, 2945, and 2982 cm^{-1} are assigned to the C–H stretching vibrations of methanol.[36] A large and broad peak at 3323 cm^{-1} in the spectra of the $C_{12}mim^+TFSA^-$–CH_3OH solutions is assigned to the O–H stretching vibration ν_{HB} of hydrogen-bonded methanol molecules. A small peak at 3562 cm^{-1} observed in the spectra of the solutions is ascribed to the O–H stretching vibration ν_I of isolated methanol molecules. Thus, methanol molecules exist in two different states, the isolated and hydrogen-bonded molecules, in the ILs. This is in agreement with the previous report on methanol solutions of $C_2mim^+BF_4^-$, $C_4mim^+BF_4^-$, and $C_4mim^+PF_6^-$.[37]

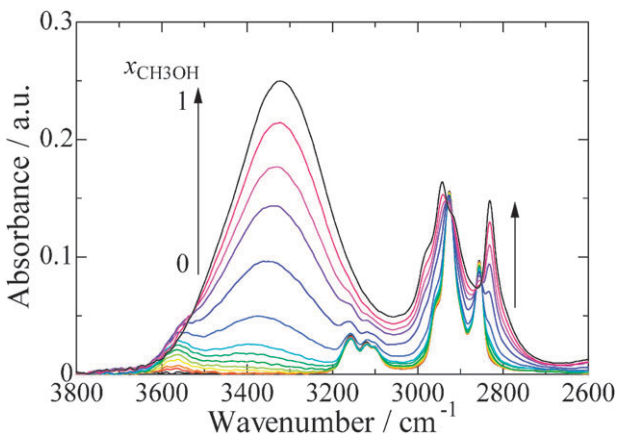

Fig. 4 ATR-IR spectra of $C_{12}mim^+TFSA^-$–CH_3OH solutions at various x_{CH_3OH}. The arrows indicate the increase in the x_{CH_3OH}.

To estimate the concentrations of both isolated and hydrogen-bonded methanol molecules, the two peaks at 3562 and 3323 cm^{-1} were fitted using a pseudo-Voigt function consisting of Lorentzian and Gaussian to deconvolute them into each component. Then, the amounts of the isolated and hydrogen-bonded methanol molecules were estimated from the areas of the ν_I and ν_{HB} bands, respectively. The molar absorption coefficient of the ν_I band was first determined from the spectrum of the $C_n mim^+TFSA^-$–CH_3OH solution at $x_{CH_3OH} = 0.1$ on the approximation that no methanol molecules form hydrogen bonds with themselves. Indeed, the area of the ν_{HB} band at the mole fraction is negligible. The concentrations of the isolated methanol molecules of the solutions at the other methanol mole fractions were then estimated from the area of the ν_I band using the molar absorption coefficient determined. In contrast, the concentrations of the hydrogen-bonded methanol molecules were obtained by subtracting the concentration of the isolated methanol molecules from that of the total methanol molecules.

Fig. 5 shows the concentrations of the isolated and hydrogen-bonded methanol molecules of the $C_n mim^+TFSA^-$–CH_3OH solutions as a function of x_{CH_3OH}. The significant alkyl-chain length dependence is not observed in the change in each concentration with increasing x_{CH_3OH}. The concentrations of the isolated methanol molecules of all the solutions increase to $\sim$2.0 mol dm^{-3} as the x_{CH_3OH} increases to 0.8, but drastically decrease with further increasing x_{CH_3OH}. Thus, an

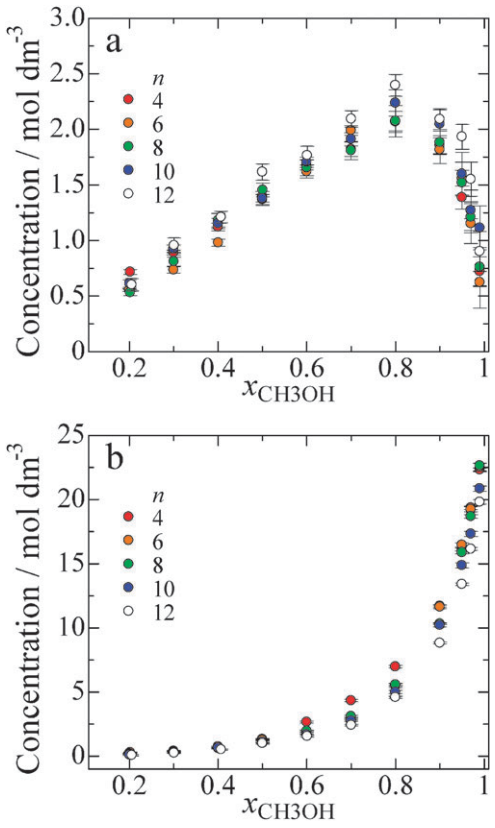

Fig. 5 Molarities of (a) isolated and (b) hydrogen-bonded methanol molecules of $C_n mim^+TFSA^-$–CH_3OH solutions as a function of x_{CH_3OH}. The standard deviations σ are indicated as error bars.

inflection point appears at $x_{CH_3OH} \approx 0.8$. The concentrations of the hydrogen-bonded methanol molecules gently increase with increasing x_{CH_3OH} to $\sim$0.7. However, those conspicuously increase with increasing x_{CH_3OH} from $\sim$0.7 to 0.99, resulting in an inflection point at $x_{CH_3OH} \approx 0.8$. The inflection point at $x_{CH_3OH} \approx 0.8$ in both concentrations agrees with the results of the SANS measurements; the significant SANS intensities of the solutions begin to appear at $x_{CH_3OH} \approx 0.8$. This coincidence strongly suggests the significant change in the mixing state of the $C_n mim^+ TFSA^-$–methanol solution at $x_{CH_3OH} \approx 0.8$. As seen in Fig. 5, in the range of $x_{CH_3OH} < \sim 0.8$ the concentrations of the hydrogen-bonded methanol are comparable with those of the isolated molecules. Thus, methanol molecules exist as both isolated and hydrogen-bonded molecules, such as dimers, in the inherent structure of $C_n mim^+ TFSA^-$. On the other hand, in the range of $x_{CH_3OH} > \sim 0.8$ the concentrations of the hydrogen-bonded methanol become much higher than those of the isolated ones; *i.e.*, most of the methanol molecules form aggregates by the hydrogen bonds among them in the solutions. Thus, the heterogeneity of the $C_n mim^+ TFSA^-$–methanol solutions observed by the SANS experiments arises from the growth of methanol clusters by hydrogen bonding in the solutions.

Fig. 5 reveals that the change in the state of methanol molecules with increasing x_{CH_3OH} is almost independent of the alkyl-chain length of $C_n mim^+$. However, the molarities of both isolated and hydrogen-bonded methanol molecules depend on the different molar volumes of the $C_n mim^+ TFSA^-$. In Fig. 6, thus, the ratios of the concentrations of the isolated and hydrogen-bonded methanol to the total concentration of methanol are replotted against x_{CH_3OH}. The changes of both ratios with increasing x_{CH_3OH} are still almost independent of the alkyl-chain length of the ILs, although the difference among the ratios at each x_{CH_3OH} becomes larger in the lower mole fraction range. In particular, the ratios of the hydrogen-bonded methanol molecules overlap among them above $x_{CH_3OH} \approx 0.8$.

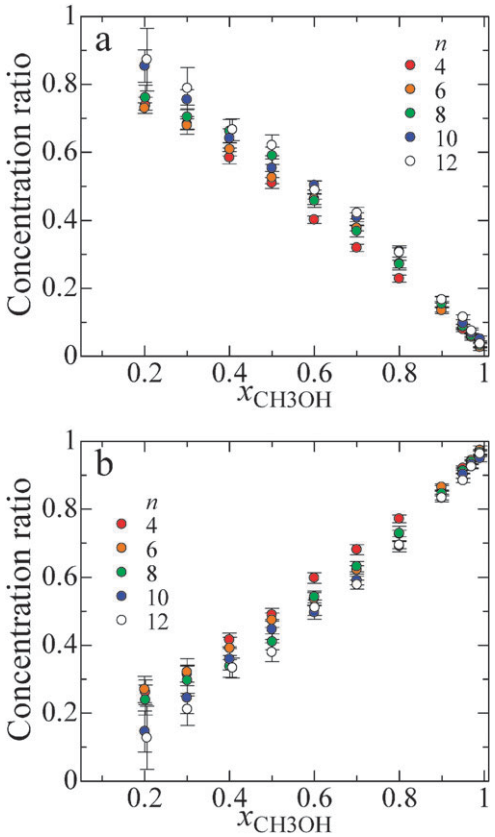

Fig. 6 Ratios of the concentrations of (a) isolated and (b) hydrogen-bonded methanol molecules to the total concentration of methanol of $C_n mim^+ TFSA^-$–CH_3OH solutions as a function of x_{CH_3OH}. The standard deviations σ are indicated as error bars.

^{1}H and ^{13}C NMR chemical shifts

Fig. 7 and 8 display ^{1}H and ^{13}C NMR chemical shifts of the $C_n mim^+ TFSA^-$–CH_3OH solutions as a function of x_{CH_3OH}, respectively. The hydroxyl hydrogen atom of methanol in all of the $C_n mim^+ TFSA^-$–CH_3OH solutions is strongly deshielded with increasing x_{CH_3OH} (Fig. 7). The change in the chemical shift of the methanol hydroxyl hydrogen with increasing x_{CH_3OH} is almost independent of the alkyl-chain length of the ILs, as well as the ATR-IR results. Thus, the growth of the hydrogen bonds among methanol molecules does not significantly depend on the alkyl-chain length of the ILs. The methyl carbon atom is shielded with increasing x_{CH_3OH}. This is caused by the hydrogen bonds of the hydroxyl group. In general, a hydrogen atom of a molecule becomes more positive by hydrogen bonding with other molecules.[28] Thus, the shielding of the methanol methyl carbon with increasing x_{CH_3OH} may arise from a flow of electrons from the hydroxyl group to the methyl carbon. In the changes in the chemical shifts of the methyl hydrogen and carbon atoms of methanol with increasing x_{CH_3OH}, an inflection point appears

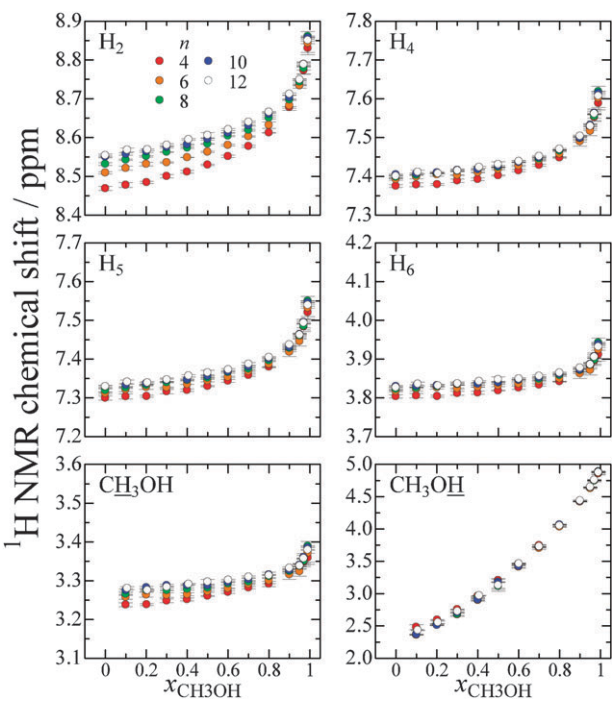

Fig. 7 ^{1}H NMR chemical shifts of $C_n mim^+ TFSA^-$–CH_3OH solutions as a function of x_{CH_3OH}. The standard deviations σ are indicated as error bars.

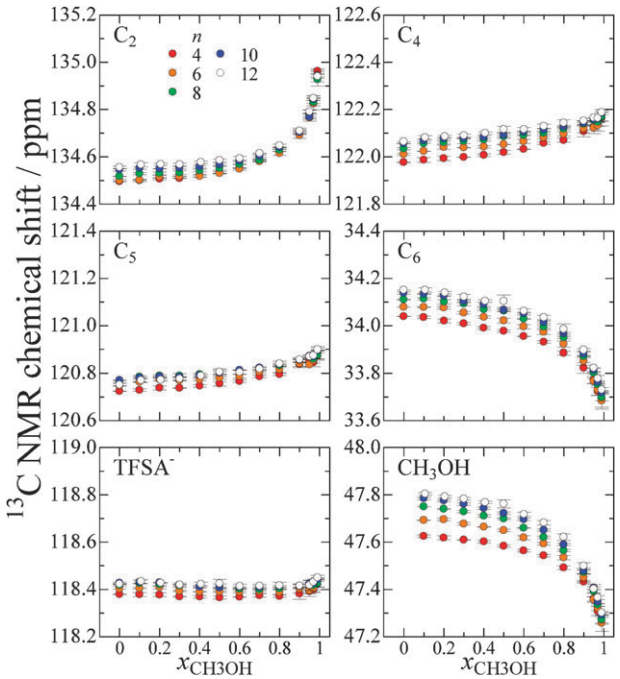

Fig. 8 ^{13}C NMR chemical shifts of $C_n$mim$^+$TFSA$^-$–CH_3OH solutions as a function of x_{CH_3OH}. The standard deviations σ are indicated as error bars.

at $x_{CH_3OH} \approx 0.8$, whereas that of the chemical shifts of the hydroxyl hydrogen atoms is indistinct. This may be attributed to the influence of the structural change of the ILs on the methanol methyl group because the methyl group is allowed to orientate toward the outside of methanol clusters by hydrogen bonding. In contrast, the values of the methanol hydroxyl hydrogen are given as the weighted averages of the chemical shifts for the isolated and hydrogen-bonded molecules.

In all the $C_n$mim$^+$TFSA$^-$–CH_3OH solutions, the imidazolium and methyl hydrogen atoms of the cations are moderately deshielded with increasing x_{CH_3OH} to $\sim$0.8. The deshielding of the hydrogen atoms becomes more remarkable above $x_{CH_3OH} \approx 0.8$. This results in an inflection point at $x_{CH_3OH} \approx 0.8$. The inflection point at $x_{CH_3OH} \approx 0.8$ is in agreement with the results of the SANS and ATR-IR measurements. The same tendency is shown in the shifts of the imidazolium carbon atoms. The NMR results reveal that the inherent structure of ILs around the imidazolium ring drastically changes at $x_{CH_3OH} \approx 0.8$. The significant deshielding of the imidazolium hydrogen and carbon atoms above $x_{CH_3OH} \approx 0.8$ may be ascribed to interaction between the imidazolium hydrogen atoms and methanol, such as weak C–H$\cdots$O hydrogen bond due to the increase in the methanol content. In fact, the changes in the chemical shifts of the most positive H_2 and C_2 atoms with increasing x_{CH_3OH} are more significant compared to the other atoms.[38,39] However, the methyl carbon C_6 atom is shielded with increasing x_{CH_3OH}. This may be because the electrons of the imidazolium ring flow to the C_6 atom due to the weak C–H$\cdots$O hydrogen bonds.

Interestingly, the ^{1}H and ^{13}C chemical shifts of the imidazolium cation and the methanol methyl group at each mole fraction in the range of $x_{CH_3OH} < 0.8$ depend on the alkyl-chain length. For instance, the chemical shift of the H_2 atom at each mole fraction is larger in the order of the chain length from $n = 4$ to 12. In contrast, the chemical shifts of all the solutions almost overlap among them in the range of $x_{CH_3OH} > \sim 0.8$. A similar tendency is observed in the O–H vibrations of the ATR-IR results (Fig. 6). The inherent structure of $C_n$mim$^+$TFSA$^-$ with different alkyl-chain lengths may cause the order of the chemical shifts of $C_n$mim$^+$ below $x_{CH_3OH} \approx 0.8$. The formation of the hydrogen bonds among methanol molecules may be weakly affected by the inherent structure of the ILs. However, the structure of $C_n$mim$^+$TFSA$^-$ is gradually loosened in the solutions above $x_{CH_3OH} \approx 0.8$. The imidazolium hydrogen atoms often interact with methanol due to the increase in the methanol content. The interaction between the imidazolium hydrogen atoms and methanol is not largely different among the $C_n$mim$^+$ with n = 4–12. Thus, the ^{1}H and ^{13}C chemical shifts of the imidazolium cation and methanol do not depend on the alkyl-chain length of $C_n$mim$^+$ above $x_{CH_3OH} \approx 0.8$.

In contrast to $C_n$mim$^+$ and methanol, the chemical shift of trifluoromethyl carbon atoms of TFSA$^-$ hardly changes against the increase in the methanol mole fraction to $x_{CH_3OH} \approx 0.9$. Above $x_{CH_3OH} \approx 0.9$, the TFSA$^-$ carbon atoms are slightly deshielded. The previous investigation on the inherent structure of C_2mim$^+$TFSA$^-$ by large-angle X-ray scattering technique and MD simulations shows that the H_2, H_4, and H_5 atoms of C_2mim$^+$ interact with the oxygen atoms of the –$SO_2(CF_3)$ groups of TFSA$^-$.[40] Thus, the constant values of the trifluoromethyl carbon atoms below $x_{CH_3OH} \approx 0.9$ suggest that the interactions between the TFSA$^-$ oxygen atom and the imidazolium hydrogen atoms are kept in the solutions. However, the deshielding of the carbon atoms above $x_{CH_3OH} \approx 0.9$ is ascribed to the replacement of TFSA$^-$ at the imidazolium hydrogen atoms by methanol and the solvation of TFSA$^-$ by methanol.

Effects of the alkyl-chain length

On the basis of the results from the SANS, ATR-IR, and NMR measurements, the mixing state of the $C_n$mim$^+$TFSA$^-$–methanol solutions with increasing x_{CH_3OH} can be concluded as below. In the range of $x_{CH_3OH} < \sim 0.8$, the inherent structure of $C_n$mim$^+$TFSA$^-$ is kept in the solutions. The concentration of hydrogen-bonded methanol molecules conspicuously increases in the solutions above $x_{CH_3OH} \approx 0.8$. The SANS results reveal that the heterogeneity of the $C_n$mim$^+$TFSA$^-$–methanol solutions becomes significant at $x_{CH_3OH} \approx 0.8$. This is due to the growth of methanol clusters by hydrogen bonding in the IL structure. The heterogeneity of the solutions is most notably enhanced at $x_{CD_3OD} \approx 0.97$ over the entire range. Interestingly, these two mole fractions of the $C_n$mim$^+$TFSA$^-$–methanol solutions are independent of the alkyl-chain length of $C_n$mim$^+$, except for C_4mim$^+$. Moreover, the variations in the concentrations of the isolated and hydrogen-bonded methanol molecules estimated by the ATR-IR measurements and the NMR chemical shifts with increasing x_{CH_3OH} do not remarkably depend on the alkyl-chain length. We consider a plausible reason for these features of the $C_n$mim$^+$TFSA$^-$–methanol solutions as follows.

As shown by the previous MD investigation,[12] the imidazolium rings and $TFSA^-$ may aggregate with themselves to form the polar domains in $C_n mim^+TFSA^-$, while the alkyl chains interact among them to form the nonpolar domains. In the solutions, methanol clusters by hydrogen bonding may be formed mainly in the polar domains of $C_n mim^+TFSA^-$ because methanol is a polar molecule. The Ornstein–Zernike behaviour of the SANS spectra of the solutions suggests that methanol clusters do not have a definite shape like a micelle in the solutions. They are spinodally evolved in the inherent structure of the ILs with increasing x_{CH_3OH} to enhance the concentration fluctuation of the $C_n mim^+TFSA^-$–methanol solutions.[32] This is the same as the increase in the heterogeneity of binary solutions of molecular liquids, such as acetonitrile–water[41] and 1,4-dioxane–water solutions.[42] In the range of $x_{CH_3OH} < \sim 0.8$, methanol clusters are not remarkably evolved in the $C_n mim^+TFSA^-$–methanol solutions due to the small volume ratio of methanol ($\phi_{CH_3OH} \approx 0.3$). Thus, the inherent structure of $C_n mim^+TFSA^-$ is not significantly disrupted in this x_{CH_3OH} range. This is proved by the alkyl-chain length dependence of the ^1H and ^{13}C NMR in the range of $x_{CH_3OH} < \sim 0.8$. As shown by the ATR-IR measurements, methanol molecules exist as isolated molecules and small aggregates such as dimers in the ILs, but do not strongly interact with the imidazolium ring and $TFSA^-$ because of absence of sites of strong hydrogen bonding within both ions. Hence, the mixtures of the ILs and methanol cannot be considered as homogeneous solutions even in the range of $x_{CH_3OH} < \sim 0.8$. However, methanol clusters notably grow in the polar domains with further increasing of x_{CH_3OH} from ~ 0.8. Thus, the microphase separation between the polar and nonpolar domains in the ILs progresses more as the x_{CH_3OH} increases. The strengthening of the SANS intensities of the $C_n mim^+TFSA^-$–CD_3OD solutions is attributed to the contrast between the polar domains that involve CD_3OD clusters and the nonpolar domains of the alkyl groups. The aggregation of methanol molecules is mainly affected by the polar domain of ILs but not by the nonpolar domain of the alkyl chains. The properties of the polar domains, particularly the electrostatic force, are not largely different among all the $C_n mim^+TFSA^-$ studied, as discussed in the NMR results. This is the reason why the mole fraction at the maximum heterogeneity of the $C_n mim^+TFSA^-$–methanol solutions does not remarkably depend on the alkyl-chain length.

However, the maximum correlation length ξ of the solutions at $x_{CD_3OD} \approx 0.97$ becomes larger in the order of the alkyl-chain length from $n = 6$ to 12. This is because the longer the alkyl group, the larger the nonpolar domains that are formed in $C_n mim^+TFSA^-$.[12] The shortest alkyl chain of $C_4 mim^+TFSA^-$ shows that the correlation length ξ reaches the maximum at the lower mole fraction of $x_{CD_3OD} \approx 0.95$ compared to the other ILs. This arises from the blurred microphase separation of $C_4 mim^+TFSA^-$ due to the short alkyl chain.

As the mole fraction further increases beyond the maximum of the heterogeneity, the interactions between $C_n mim^+$ and $TFSA^-$ in the polar domains may be loosened in the solutions due to the solvation of both ions by the larger number of methanol molecules. In fact, the ^1H and ^{13}C NMR data of the imidazolium cations reveal the solvation of the imidazolium ring by methanol. Moreover, the deshielding of the carbon atoms of $TFSA^-$ observed by the ^{13}C NMR measurements suggests the replacement of $TFSA^-$ at the imidazolium hydrogen atoms by methanol and the solvation of $TFSA^-$. The electrostatic interaction between $C_n mim^+$ and $TFSA^-$ is weakened, and then the repulsive force begins to act between the imidazolium rings in the polar domains. This leads to the loosening of the interaction between the alkyl groups in the nonpolar domains. Thus, the heterogeneous mixing between $C_n mim^+TFSA^-$ and methanol becomes weaker, resulting in the decrease in the correlation lengths ξ of the $C_n mim^+TFSA^-$–CD_3OD solutions at $x_{CD_3OD} = 0.99$. This loosening process of the polar and nonpolar domains of the ILs with increasing methanol mole fraction agrees with the previous expectation on IL–water solutions from the MD simulations.[16]

The structural change of all the $C_n mim^+TFSA^-$–methanol solutions begins at $x_{CH_3OH} \approx 0.8$, as shown by the ATR-IR and NMR results. This may be attributed to the three sites of weak C–H$\cdots$O hydrogen bonds between the imidazolium ring and methanol. Thus, three methanol molecules are necessary to occupy the sites of the imidazolium ring, corresponding to $x_{CH_3OH} = 0.75$. In practice, however, more than three methanol molecules are needed to interact with the imidazolium hydrogen atoms due to the equilibrium of the weak hydrogen bonds between them. This leads to the delayed inflection points at $x_{CH_3OH} \approx 0.8$ and 0.9 in the ATR-IR and NMR data of $C_n mim^+$ and $TFSA^-$, respectively.

4. Conclusion

The SANS results on the $C_n mim^+TFSA^-$–methanol solutions revealed that methanol is heterogeneously mixed with the $C_n mim^+TFSA^-$ in the range of $0.8 \leq x_{CD_3OD} \leq 0.995$. The maximum heterogeneity of the solutions appeared at $x_{CD_3OD} \approx 0.97$, except for $C_4 mim^+TFSA^-$. Additionally, the ATR-IR and NMR results revealed that the mixing state of the $C_n mim^+TFSA^-$–methanol solutions changes with increasing x_{CH_3OH} in the same way among the ILs studied. In the solutions above $x_{CH_3OH} \approx 0.8$, particularly, the changes in the interactions of $C_n mim^+$–methanol, $TFSA^-$–methanol, and methanol–methanol with methanol content do not depend on the alkyl-chain length of the $C_n mim^+$. The aggregation of methanol molecules by hydrogen bonding is mainly affected by both $C_n mim^+$ and $TFSA^-$, but not by the alkyl chain. Thus, the SANS intensities of the solutions are due to the contrast between the polar domains including $C_n mim^+$, $TFSA^-$, and methanol clusters and the nonpolar domains of the alkyl chains. The present investigation thus demonstrated the microphase separation between the polar domains and nonpolar domains of $C_n mim^+TFSA^-$ as expected from the MD simulations.[14,15] In addition, the decrease in the SANS intensities of the solutions above $x_{CD_3OD} \approx 0.97$, together with the NMR results on the interactions of $C_n mim^+$–methanol and $TFSA^-$–methanol, corroborated the loosening of the polar and nonpolar domains expected also by the MD simulations.[16]

Acknowledgements

This work was supported partly by Grants-in-Aid (No. 199550022 and 22550018) from the Japan Society for the Promotion of Science. The SANS experiments were carried out in joint research with the Institute for Solid State Physics, the University of Tokyo (Proposal No. 8851). The density and NMR measurements for the sample solutions were conducted at the Analytical Research Centre for Experimental Sciences of Saga University.

References

1 M. J. Earle and K. R. Seddon, *Pure Appl. Chem.*, 2000, **72**, 1391.
2 K. N. Marsh, J. A. Boxall and R. Lichtenthaler, *Fluid Phase Equilib.*, 2004, **219**, 93.
3 S. Pandey, *Anal. Chim. Acta*, 2006, **556**, 38.
4 J. Li, Y. Cai, Y. Shi, S. Mou and G. Jiang, *Talanta*, 2008, **74**, 498.
5 J. Liu, J. A. Jonsson and G. Jiang, *TrAC, Trends Anal. Chem.*, 2005, **24**, 20.
6 J. L. Anderson, D. W. Armstrong and G. Wei, *Anal. Chem.*, 2006, **78**, 2893.
7 T. Shimomura, M. Tabata and J. Nishimoto, *J. Porphyrins Phthalocyanines*, 2009, **13**, 849.
8 W. Li, Z. Zhang, J. Zhang, B. Han, B. Wang, M. Hou and Y. Xie, *Fluid Phase Equilib.*, 2006, **248**, 211.
9 M. Koeberg, C. Wu, D. Kim and M. Bonn, *Chem. Phys. Lett.*, 2007, **439**, 60.
10 W. Liu, T. Zhao, Y. Zhang, H. Wang and M. Yu, *J. Solution Chem.*, 2006, **35**, 1337.
11 J. Wang, H. Wang, S. Zhang, H. Zhang and Y. Zhao, *J. Phys. Chem. B*, 2007, **111**, 6181.
12 J. N. A. C. Lopes and A. A. H. Pádua, *J. Phys. Chem. B*, 2006, **110**, 3330.
13 A. Triolo, O. Russina, H.-J. Bleif and E. D. Cola, *J. Phys. Chem. B*, 2007, **111**, 4641.
14 J. N. C. Lopes, M. F. C. Gomes and A. A. H. Pádua, *J. Phys. Chem. B*, 2006, **110**, 16816.
15 A. A. H. Pádua, M. F. C. Gomes and J. N. A. C. Lopes, *Acc. Chem. Res.*, 2007, **40**, 1087.
16 W. Jiang, Y. Wang and G. A. Voth, *J. Phys. Chem. B*, 2007, **111**, 4812.
17 J. Bowers, C. P. Butts, P. J. Martin, M. C. Vergara-Gutierrez and R. K. Heeman, *Langmuir*, 2004, **20**, 2191.
18 T. Singh and A. Kumar, *J. Phys. Chem. B*, 2007, **111**, 7843.
19 L. Gallon, J. Sirieix-Plenet and P. Letellier, *J. Solution Chem.*, 2004, **33**, 1333.
20 Y. Zhao, S. Gao, J. Wang and J. Tang, *J. Phys. Chem. B*, 2008, **112**, 2031.
21 J. M. Crosthwaite, S. N. V. K. Aki, E. J. Maginn and J. F. Brennecke, *J. Phys. Chem. B*, 2004, **108**, 5113.
22 A. Heintz, J. K. Lehmann, C. Wertz and J. Jacquemin, *J. Chem. Eng. Data*, 2005, **50**, 956.
23 T. Takamuku, Y. Honda, K. Fujii and S. Kittaka, *Anal. Sci.*, 2008, **24**, 1285.
24 P. Nockemann, K. Binnemans and K. Driesen, *Chem. Phys. Lett.*, 2005, **415**, 131.
25 S. Okabe, M. Nagao, T. Karino, S. Watanabe, T. Adachi, H. Shimizu and M. Shibayama, *J. Appl. Crystallogr.*, 2005, **38**, 1035.
26 S. Okabe, T. Karino, M. Nagao, S. Watanabe and M. Shibayama, *Nucl. Instrum. Methods Phys. Res., Sect. A*, 2007, **572**, 853.
27 J. E. Bertie and H. H. Eysel, *Appl. Spectrosc.*, 1985, **39**, 392.
28 K. Mizuno, Y. Tamiya and M. Mekata, *Pure Appl. Chem.*, 2004, **76**, 105.
29 K. Mizuno, S. Imafuji, T. Ochi, T. Ohta and S. Maeda, *J. Phys. Chem. B*, 2000, **104**, 11001.
30 K. Momoki and Y. Fukazawa, *Anal. Chem.*, 1990, **62**, 1665.
31 K. Momoki and Y. Fukazawa, *Anal. Sci.*, 1994, **10**, 53.
32 L. Almásy, M. Turmine and A. Perera, *J. Phys. Chem. B*, 2008, **112**, 2382.
33 E. R. Talaty, S. Raja, V. J. Storhaug, A. Dolle and W. R. Carper, *J. Phys. Chem. B*, 2004, **108**, 13177.
34 R. W. Berg, M. Deetlefs, K. R. Seddon, I. Shim and J. M. Thompson, *J. Phys. Chem. B*, 2005, **109**, 19018.
35 J. Kiefer, J. Fries and A. Leipertz, *Appl. Spectrosc.*, 2007, **61**, 1306.
36 Y. J. Hu, H. B. Fu and E. R. Bernstein, *J. Chem. Phys.*, 2006, **125**, 154306.
37 M. L. Lopez-Pastor, M. J. Ayora-Canada, M. Valcarcel and B. Lendl, *J. Phys. Chem. B*, 2006, **110**, 10896.
38 A. Elaiwi, P. B. Hitchcock, K. R. Seddon, N. Srinivasan, Y.-M. Tan, T. Welton and J. A. Zora, *J. Chem. Soc., Dalton Trans.*, 1995, 3467.
39 C. Hardacre, J. D. Holbrey, S. E. J. McMath, D. T. Bowron and A. K. Soper, *J. Chem. Phys.*, 2003, **118**, 273.
40 K. Fujii, Y. Soejima, Y. Kyoshoin, S. Fukuda, R. Kanzaki, Y. Umebayashi, T. Yamaguchi, S. Ishiguro and T. Takamuku, *J. Phys. Chem. B*, 2008, **112**, 4329.
41 T. Takamuku, Y. Noguchi, M. Matsugami, H. Iwase, T. Otomo and M. Nagao, *J. Mol. Liq.*, 2007, **136**, 147.
42 T. Takamuku, A. Nakamizo, M. Tabata, K. Yoshida, T. Yamaguchi and T. Otomo, *J. Mol. Liq.*, 2003, **103–104**, 143.

